

Modeling same-order modes of multicell cavities

Olof Troeng*

Department of Automatic Control, Lund University, Sweden

(Dated: February 11, 2021)

We derive the transfer function of a multicell cavity with parasitic same-order modes (from power coupler to pickup probe). The derived model is discussed and compared to measurement data.

I. INTRODUCTION

Multicell elliptical cavities are suitable for accelerating particle beams with velocities greater than $0.5c$. However, these cavities intrinsically have parasitic electromagnetic modes that are close in frequency to the accelerating mode. These so-called *same-order modes*, or fundamental passband modes, interact both with the rf system and the beam. Their interaction with the rf system may, without counter-measures, give instability in the field control loop [1], and their interaction with the beam drives emittance growth [2]. Dynamic models of same-order modes and these interactions are necessary for design and analysis of field control algorithms.

The regular geometry of multicell elliptical cavities makes it possible to derive the same-order-mode dynamics from a small number of cavity parameters. Such dynamic models have been used for studying how beating of same-order modes affects the beam [3]. The steady-state models in [4–7] capture the shapes and resonance frequencies of the modes but not their dynamics and decay rates.

For field control analysis in the frequency domain, it is necessary to know the transfer function from the rf drive to the pickup-probe signal. In [1], a real-coefficient, two-input two-output transfer function from rf drive to pickup signal (valid for superconducting cavities) was presented without motivation. Such real-coefficient, two-input two-output models are common in the field control literature. However, as we discussed in [8], the equivalent, complex-coefficient, single-input single-output (SISO) representation gives more intuition and simplifies analysis.

In this paper we: (1) derive a complex baseband model of a multicell cavity along the lines of [3], but using the energy-based parameterization from [9]; (2) normalize that model to make it suitable for field control analysis; (3) derive the complex-coefficient SISO transfer function from power coupler to pickup signal (also valid for normal-conducting cavities); and (4) fit the transfer-function model to measurement data from a 6-cell niobium cavity taken at room temperature and cryogenic temperature.

Remark 1: An incorrect transfer-function model for cavities with parasitic modes was proposed in [10]. It was based on taking the transfer function of the individual modes from [1] and multiplying them with the modes' coupling strengths to the rf system, although that effect

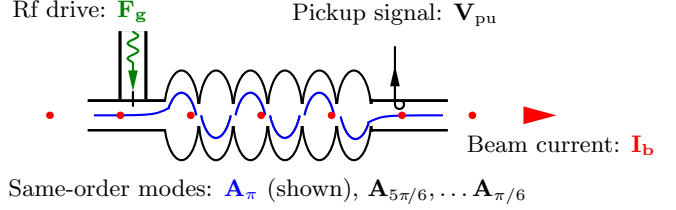


FIG. 1. Schematic of 6-cell elliptical cavity. Power is fed through the power coupler in the leftmost cell and the cavity field is sensed by a pickup probe in the rightmost cell.

was already accounted for in [1]. The incorrect model in [10] predicts that the resonance peaks have different magnitudes, while both the analysis in this paper and [11][Fig. 5.9] indicate that they have similar magnitudes.

Also the stability analysis in [10] is problematic. It is not possible to analyze closed-loop stability of MIMO systems with strong cross couplings (as from same-order modes) using loop-by-loop analysis [12, Sec. 8.6], [13]. The complex-signal perspective in [8] together with the model in this paper enables correct and intuitive analysis.

II. SAME-ORDER MODES OF MULTICELL CAVITIES

A. Cavity model with parasitic modes

We start by considering parasitic modes of a general cavity using the energy-based parameterization in [9, 14]. Let \mathbf{A}_k be the complex envelope of mode k , with its magnitude (units $\sqrt{\text{J}}$) scaled so that $|\mathbf{A}_k|^2$ is the mode energy. This unambiguously defines the mode amplitude without reference to the effective voltage of the accelerating mode. If coupling between the modes can be neglected then their complex envelopes evolve according to [9]

$$\frac{d\mathbf{A}_k}{dt} = (-\gamma_k + i\Delta\omega_k)\mathbf{A}_k + \sqrt{2\gamma_{\text{ext}k}}\mathbf{F}_g + \frac{\alpha_k}{2}\mathbf{I}_b, \quad (1a)$$

where $\gamma_k = \gamma_{0k} + \gamma_{\text{ext}k}$ is the decay rate of the mode amplitudes (γ_{0k} corresponds to resistive losses and $\gamma_{\text{ext}k}$ to decay through the power coupler); $\Delta\omega_k = \omega_k - \omega_{\text{rf}}$ is the offset of the mode frequency ω_k relative to the nominal rf frequency ω_{rf} ; \mathbf{F}_g (units $\sqrt{\text{W}}$) is the envelope of the forward wave from the rf amplifier with $|\mathbf{F}_g|^2$ equal to the power in the wave; and \mathbf{I}_b is the beam phasor, with $|\mathbf{I}_b|$ equal to the dc beam current. The complex envelopes

* E-mail: oloft@control.lth.se

\mathbf{A}_k are defined relative to ω_{rf} , with their phases chosen so that the coefficients in front of \mathbf{F}_g are real. The voltage sensed by the pickup probe is a linear combination

$$\mathbf{V}_{\text{pu}} = \sum_{k=a,1,2,\dots}^N \mathbf{C}_k \mathbf{A}_k \quad (1b)$$

of the mode amplitudes, where \mathbf{C}_k are complex coefficients. Here we have used the subscript a to indicate the mode intended for acceleration. We will use a different labeling when discussing same-order modes.

The cavity-beam-coupling parameters α_k are in general complex. However, the parameter $\alpha_a = \alpha_a$ for the accelerating mode is real due to the definition of \mathbf{I}_b .

Normalized model with parasitic modes

In many situations, e.g., field control analysis, it is easier to work with normalized models. Therefore, we introduce the following dimension-free, normalized variables similarly to in [9],

$$\mathbf{a}_k := \frac{1}{A_{a0}} \mathbf{A}_k \quad (2a)$$

$$\mathbf{f}_g := \frac{1}{\gamma_a A_{a0}} \sqrt{2\gamma_{\text{ext}a}} \mathbf{F}_g \quad (2b)$$

$$\mathbf{i}_b := \frac{1}{\gamma_a A_{a0}} \frac{\alpha_a}{2} \mathbf{I}_b \quad (2c)$$

$$\mathbf{v}_{\text{pu}} := \frac{1}{C_a A_{a0}} \mathbf{V}_{\text{pu}}, \quad (2d)$$

where A_{a0} is the nominal magnitude of the accelerating mode. With the variables (2) we can write (1) as

$$\frac{d\mathbf{a}_k}{dt} = (-\gamma_k + i\Delta\omega_k)\mathbf{a}_k + \gamma_a \frac{\sqrt{2\gamma_{\text{ext}k}}}{\sqrt{2\gamma_{\text{ext}a}}} \mathbf{f}_g + \gamma_a \frac{\alpha_k}{\alpha_a} \mathbf{i}_b. \quad (3a)$$

$$\mathbf{v}_{\text{pu}} = \mathbf{a}_a + \sum_{k=1,2,\dots}^N \mathbf{c}_k \mathbf{a}_k \quad (3b)$$

where $\mathbf{c}_k := \mathbf{C}_k / (C_a A_{a0})$. The normalization (3) has the nominal operating point $\mathbf{a}_a = 1$ and the steady-state sensitivity of \mathbf{a}_a to variations in \mathbf{f}_g and \mathbf{i}_b is unity.

B. Same-order modes of multicell elliptical cavities

The same-order modes of a multicell cavity arise from the coupling between the cells' fundamental modes, similarly as for a chain of weakly coupled oscillators. An N -cell cavity has N closely spaced same-order modes. The parameters in (3) of these modes, can, due to the regular cavity geometry, be computed from a small number of basic cavity parameters, as shown in the Appendix. The modes are conventionally referred to as the π/N mode,

TABLE I. Values of R_n^2 for different n and N , see (4) for R_n .

N	n								
	9	8	7	6	5	4	3	2	1
5					1	1.81	1.31	0.69	0.19
6				1	1.87	1.50	1.00	0.50	0.13
9	1	1.94	1.77	1.50	1.17	0.83	0.50	0.23	0.06

the $2\pi/N$ mode, up to the π mode. This naming indicates the cell-to-cell phase advance of the *sinusoidal envelope of the mode shapes*¹. It is typically the π mode that is used as the accelerating mode [5]. We will use a subscript π to indicate parameters of the π mode and a subscript n for the $n\pi/N$ mode.

The derivation in the appendix assumes an ‘‘ideal’’ N -cell cavity in that: all cell-to-cell coupling factors equal k_{cc} ; all inner-cells have resonance frequencies equal to ω_{cell} ; the end-cell resonance frequencies are tuned for a flat π mode; and mode coupling is negligible. Under these assumptions, the same-order-mode parameters depend, in addition to N , ω_{cell} , and k_{cc} , only on the cell's resistive decay rate γ_0 and the decay rate γ_{pc} through the power coupler from the connected end cell. By introducing

$$R_n := \begin{cases} \sqrt{2} \sin \frac{n\pi}{2N} & \text{if } n < N \\ 1 & \text{if } n = N \end{cases}, \quad (4)$$

the parameters can be expressed as

$$\Delta\omega_n = \omega_{\text{cell}} \sqrt{1 + 2R_n^2 k_{cc}} - \omega_{\text{rf}} \quad (n < N) \quad (5)$$

$$\approx \omega_{\text{cell}} (\sqrt{1 + 2R_n^2 k_{cc}} - \sqrt{1 + 4k_{cc}}) \quad (5')$$

$$\gamma_{0n} = \gamma_0 \quad (6)$$

$$\gamma_{\text{ext}n} = R_n^2 \gamma_{\text{pc}} / N = R_n^2 \gamma_{\text{ext}\pi} \quad (7)$$

$$\mathbf{c}_n = (-1)^{N-n} R_n. \quad (8)$$

The approximation (5') assumes that $\Delta\omega_\pi = \omega_\pi - \omega_{\text{rf}}$ is small relative to $\Delta\omega_{N-1}$, see also Remark 2. With the relationships (5)–(8) the general model in (3) takes the form in Fig. 2. Values of R_n^2 for different values of N and n are shown in Table I. In the next section we investigate how well the relations (5)–(8) agree for parameters estimated from a real-world cavity.

Remark 2: While $\Delta\omega_\pi$ is negligible relative to both $\Delta\omega_{N-1}$ and typical field control bandwidths, its precise tuning, typically to a value slightly larger than 0, is crucial for minimizing the drive power $|\mathbf{F}_g|^2$ [5, 6, 9].

Remark 3: Typical cell-to-cell coupling factors k_{cc} are

¹ The cell-to-cell phase difference of the modes themselves is 0 or π .

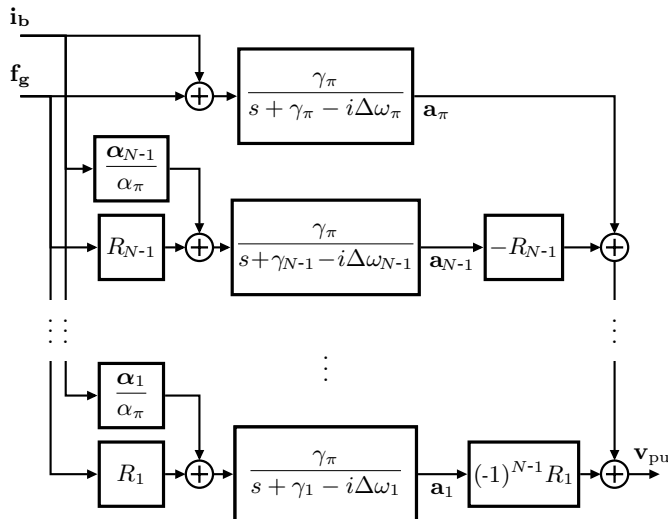


FIG. 2. Block diagram for a normalized model of a cavity with parasitic same-order modes. Subscripts n indicate the $n\pi/N$ mode.

on the order of 0.01, which gives

$$\begin{aligned} \Delta\omega_n &\approx \omega_{\text{cell}} \left(\sqrt{1 + 2R_n^2 k_{cc}} - \sqrt{1 + 4k_{cc}} \right) \\ &\approx (R_n^2 - 2)k_{cc}\omega_{\text{cell}}. \end{aligned}$$

This shows that the baseband frequencies of the same-order modes are approximately proportional to $R_n^2 - 2$.

Remark 4: There are two definitions of the cell-to-cell coupling factor k_{cc} in the accelerator literature. The *full-passband-width* definition, for which $k_{cc} \approx (\omega_\pi - \omega_1)/\omega_\pi$ [4, 6, 7, 11] and the *half-passband-width* definition [3, 5] for which k_{cc} is half as large. The first definition corresponds to the per-cycle decay of a cell’s energy due to coupling to a neighboring cell and the latter definition corresponds to the decay of the field amplitude. In this paper we use the half-passband-width definition since it gives slightly more convenient expressions.

C. Transfer function from rf drive to pickup probe

The transfer function from \mathbf{f}_g to \mathbf{v}_{pu} in Fig. 2 is important for field control analysis. It is given by

$$\begin{aligned} P_{\text{cav}}(s) &= \gamma_\pi \sum_{n=1}^N (-1)^{N-n} \frac{R_n^2}{s + \gamma_n - i\Delta\omega_n} \\ &= \frac{\gamma_\pi}{\gamma_{\text{ext}\pi}} \sum_{n=1}^N (-1)^{N-n} \frac{\gamma_{\text{ext}n}}{s + \gamma_n - i\Delta\omega_n}, \quad (9) \end{aligned}$$

where $\gamma_n := \gamma_0 + \gamma_{\text{ext}n}$ is the total decay rate of the $n\pi/N$ mode. For superconducting cavities with $\gamma_0 \ll \gamma_{\text{ext}n}$ we

have that $\gamma_{\text{ext}n} \approx \gamma_n$ and (9) simplifies to

$$P_{\text{cav}}(s) = \sum_{n=1}^N (-1)^{N-n} \frac{\gamma_n}{s + \gamma_n - i\Delta\omega_n}. \quad (10)$$

Let us observe some characteristics of the transfer function (9). First, since the numbers γ_n are small relative to the differences between the numbers $\Delta\omega_n$, the transfer function $P_{\text{cav}}(s)$ has sharp resonance peaks at (baseband) frequencies $\Delta\omega_n$. Also note that $\Delta\omega_n < 0$ for $n < N$, i.e., the baseband resonance frequencies of all parasitic same-order modes are negative.

For superconducting cavities ($\gamma_0 \ll \gamma_{\text{ext}n}$) we see from (10) that all peaks have approximately unity magnitude. For normal conducting cavities ($\gamma_0 \gg \gamma_{\text{ext}n}$) we have that the peak magnitude of the $n\pi/N$ mode equals $\gamma_{\text{ext}n}/\gamma_{\text{ext}\pi} = R_n^2$ (see Table I). Fig. 4 shows the Bode magnitude plots of these extreme cases.

III. COMPARISON TO MEASUREMENT DATA

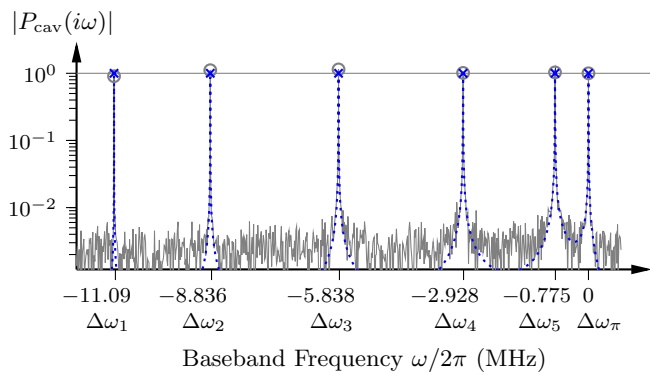
In this section we examine the fit of relationships (5)–(9) to network-analyzer measurements of a 6-cell medium- β cavity² for the European Spallation Source (ESS). Measurements were taken when the cavity was normal conducting (NC, at room temperature) and superconducting (SC, at 2 K). In the first case $\gamma_0 \gg \gamma_{\text{ext}n}$ and in the latter case $\gamma_0 \approx 0$. The measurements (scaled and frequency shifted for a unity-gain π mode at zero frequency) are shown in gray in Fig. 3.

The observed same-order-mode frequencies (relative to the π mode) are shown on the frequency axes in Fig. 3. From those values, the cell-to-cell coupling factor (half-passband-width definition) was estimated to $k_{cc} \approx 0.00862$, which makes the expression for $\Delta\omega_n$ in (5) agree with the observed frequency offsets to within $\pm 1\%$.

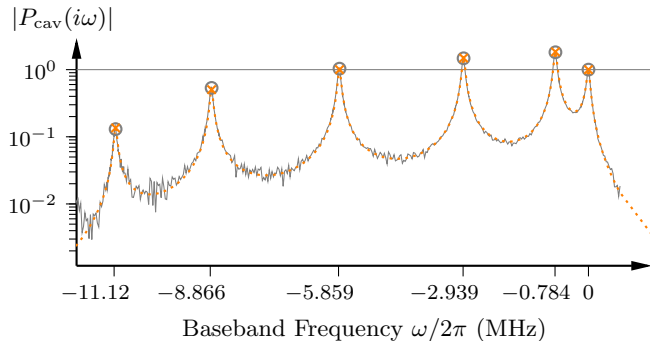
From the measurement data and the observed frequency offsets $\Delta\omega_n$, the remaining parameters in (5)–(8), namely γ_0 and $\gamma_{\text{ext}\pi}$, were estimated by fitting (9) to the data. A good fit was obtained with $\gamma_{\text{ext}\pi}/2\pi = 460$ Hz, $\gamma_0 = 0$ (SC), and $\gamma_0/2\pi = 35$ kHz (NC). Figure 3 shows the fitted models and the measurement data.

For comparison, we estimated γ_k and the peak magnitude g_k for each individual mode by fitting $g_k\gamma_k/(i(\omega - \omega_k) + \gamma_k)$ to the data in the vicinity of each mode. In Table II, these “observed” mode parameters are compared to those predicted by (6), (7), and (9). It is seen that they agree reasonably well—in particular for the modes closest to the π mode, which are the most crucial ones

² The cavity was a prototype without a tuning system, hence the mode frequencies during the measurements differed from the design frequencies. For the π -mode, which should have a nominal frequency of 704.42 MHz, the measured frequencies were 703.26 MHz (NC) and 704.24 MHz (SC). That the resonance frequency is significantly lower at room temperature is typical.



(a) Superconducting (2 K).



(b) Normal conducting (room temperature).

FIG. 3. Network-analyzer measurements of the transmission of a 6-cell ESS medium- β cavity (gray) and fits of the transfer function (9) (blue, orange). The data is scaled for unity gain of the π mode. Measurements by P. Pierini, ESS.

TABLE II. Comparison between peak magnitudes and bandwidths for measurement data and model fits in Fig. 3. The observed values are shown and the value in parenthesis indicates the deviation from the value predicted by the model.

	Superconducting		Normal conducting	
	$ P_{cav}(i\Delta\omega_k) $	$\gamma_k/2\pi$ (Hz)	$ P_{cav}(i\Delta\omega_k) $	$\gamma_k/2\pi$ (kHz)
π	1.00	450 (1.6%)	1.00	36 (-2%)
$5\pi/6$	1.03 (-3%)	870 (-2%)	1.85 (-0.2%)	35 (3%)
$4\pi/6$	1.01 (-1%)	770 (-11%)	1.49 (0.3%)	35 (3%)
$3\pi/6$	1.14 (-13%)	500 (-9%)	1.07 (-6%)	34 (3%)
$2\pi/6$	1.12 (-11%)	270 (-14%)	0.56 (-10%)	34 (5%)
$\pi/6$	0.93 (7%)	72 (-14%)	0.14 (-5%)	32 (9%)

in a field control context. The small discrepancies are probably explained by variations in the cell parameters.

For field control analysis, it is convenient to plot frequency responses using a logarithmic frequency axis, in so-called Bode diagrams. The frequency response of a normal conducting and a superconducting cavity are shown in a double-sided Bode diagram in Fig. 4. Note that superconducting cavities, whose external decay rates $\gamma_{\text{ext}\pi}$ are significantly larger than γ_0 , have resonance peaks with approximately unity magnitude (Fig. 4). For normal con-

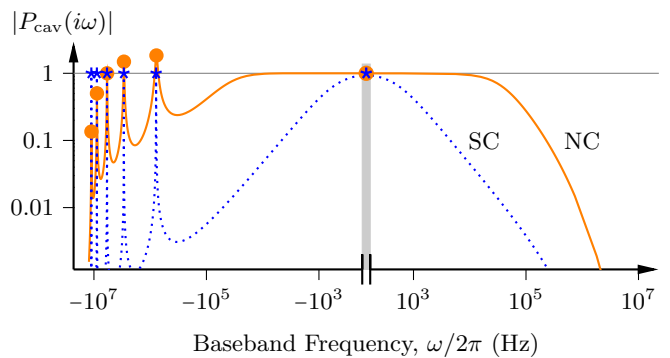


FIG. 4. Bode magnitude plots of the transfer function (9) for a 6-cell cavity when it is superconducting (SC, $\gamma_0 = 0$) and normal conducting (NC, $\gamma_0/2\pi = 35$ kHz). Note that the transfer functions have been scaled for unity magnitude at the zero frequency, see Remark 5.

ducting cavities (with small $\gamma_{\text{ext}\pi}$), the peak magnitudes are approximately given by R_n^2 .

Remark 5: Recall that the data in Fig. 3 and Fig. 4 is scaled for unity magnitude of the π mode. In absolute terms, the transmission of the normal conducting cavity is lower than for the superconducting cavity.

IV. CONCLUSION

We have derived a complex-coefficient transfer function model that is valid for both normal conducting and superconducting cavities. The model was seen to give a good fit to measurement data.

ACKNOWLEDGMENTS

Bo Bernhardsson and Paolo Pierini contributed helpful comments and suggestions. The measurement data in Sec. III was provided by Paolo Pierini. The author is a member of the ELLIIT Strategic Research Area at Lund University.

Appendix: Derivation

In this appendix, we will start from the bandpass state-space model of an N -cell cavity in [3], perform modal decomposition (diagonalization), and then transform the diagonal model to baseband.

1. Bandpass model of an N -cell cavity

Our starting point is the standard model for studying same-order modes of multicell cavities [3, 5, 7], but we

will use slightly different notation. Consider the elliptical N -cell cavity in Fig. 1 which has $N - 2$ identical inner cells and two end cells that are joined with the beam pipe. Cell 1 can be excited through a power coupler connected to the beam pipe. Adjacent cells are connected by irises that enable the propagation of the electromagnetic field. The field in cell N is sensed by a pickup probe mounted in the beam pipe.

We only consider the lowest-energy mode in each cell and we denote the electric field amplitudes of these by $x = [x_1 \cdots x_N]^T$. We assume that x_ℓ is normalized so that the squared magnitude of its complex envelope equals the energy stored in cell ℓ . Let all cell-to-cell coupling factors be given by k_{cc} ; the inner-cell resonance frequencies be given by ω_{cell} ; the end-cell resonance frequencies be given by $\omega_{\text{cell}}\sqrt{1 + 2k_{cc}}$; the rf drive (i.e., the forward wave entering the power coupler) be modeled by its complex envelope \mathbf{F}_g , with $|\mathbf{F}_g|^2$ equaling the power in the forward wave; the coupling between the waveguide and the field in cell 1 be quantified by the decay rate γ_{pc} of the field in this through the power coupler; and assume that field decay through the pickup probe is negligible. According to [3, (B-1)] the field amplitudes x in the cells evolve as a chain of weakly coupled oscillators, with the dynamics

$$\ddot{x} + 2\gamma_0\dot{x} + 2\gamma_{pc}E_1\dot{x} + \omega_{\text{cell}}^2x + \omega_{\text{cell}}^2k_{cc}Kx = 2\sqrt{2\gamma_{pc}e_1}\frac{d}{dt}\text{Re}\{\mathbf{F}_ge^{i\omega_{\text{rf}}t}\}, \quad (\text{A.1})$$

where

$$K = \begin{bmatrix} 3 & -1 & 0 & \cdots & 0 \\ -1 & 2 & -1 & 0 & \vdots \\ 0 & 0 & \ddots & & 0 \\ \vdots & & -1 & 2 & -1 \\ 0 & \cdots & 0 & -1 & 3 \end{bmatrix}, \quad (\text{A.2})$$

$$E_1 = \text{diag}(1, 0, \dots, 0),$$

$$e_1 = [1 \ 0 \ \dots \ 0]^T.$$

2. Eigenvectors and eigenvalues of the matrix K

By recalling standard trigonometric identities and doing some algebra—alternatively looking up [5, Sec. 7.2]—it can be verified that the matrix K in (A.2) has the eigenfactorization $Q\Lambda Q^T = K$, where

$$Q := \begin{bmatrix} | & | & \cdots & | \\ q_1 & q_2 & \cdots & q_N \\ | & | & \cdots & | \end{bmatrix}, \quad (\text{A.3})$$

$$\Lambda := \text{diag}(\lambda_1, \lambda_2, \dots, \lambda_N), \quad (\text{A.4})$$

and the eigenvalues λ_n are given by

$$\lambda_n = 2 \left(1 - \cos \frac{n\pi}{N}\right), \quad (\text{A.5})$$

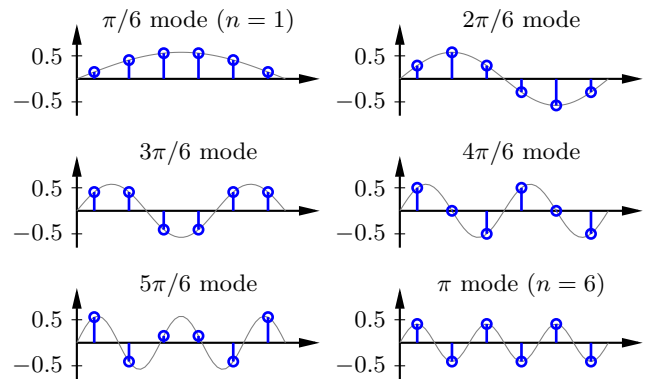


FIG. 5. Same-order-mode shapes q_n (A.6) of a 6-cell cavity.

and the orthonormal eigenvectors q_n are given by

$$q_n = \sqrt{\frac{2}{N}} \begin{bmatrix} \sin \left[\left(1 - \frac{1}{2}\right) \frac{n\pi}{N} \right] \\ \sin \left[\left(2 - \frac{1}{2}\right) \frac{n\pi}{N} \right] \\ \vdots \\ \sin \left[\left(N - \frac{1}{2}\right) \frac{n\pi}{N} \right] \end{bmatrix}, \quad q_N = \sqrt{\frac{1}{N}} \begin{bmatrix} 1 \\ -1 \\ \vdots \\ (-1)^{N-1} \end{bmatrix}. \quad (\text{A.6})$$

The mode shapes (A.6) are illustrated in Fig. 5. As mentioned in Sec. II B, mode n is often referred to as the $n\pi/N$ mode. The entries of the N th mode have equal magnitude and opposite signs and for this reason it is almost always used as the accelerating mode.

3. Diagonalizing the dynamics

Letting ξ be the passband mode amplitudes ($x = Q\xi$), we may diagonalize all of (A.1) except the third term,

$$\ddot{\xi} + 2\gamma_0\dot{\xi} + 2Q^TE_1Q\gamma_{pc}\dot{\xi} + \omega_{\text{cell}}^2(I + k_{cc}\Lambda)\xi = 2\sqrt{2\gamma_{pc}e_1}Q\frac{d}{dt}\text{Re}\{\mathbf{F}_ge^{i\omega_{\text{rf}}t}\}, \quad (\text{A.7})$$

where I is the identity matrix. For convenience, denote Q 's first row times \sqrt{N} by

$$R := \begin{bmatrix} R_1 & \cdots & R_n & \cdots & R_N \\ \sqrt{2} \sin \frac{\pi}{2N} & \cdots & \sqrt{2} \sin \frac{n\pi}{2N} & \cdots & 1 \end{bmatrix},$$

that is R_n is given by (4). Then we can write the third term of (A.7) as $2R^TR/N\gamma_{pc}\dot{\xi}$. This term, which originates from field decay through the power coupler, dynamically couples the modes. We may however assume that this interaction averages out to 0, since the beating period between the different modes is significantly shorter than the timescales at which the (complex) mode amplitudes change. Thus it suffices to keep the diagonal entries of R^TR , which correspond to the external decay rates of the modes. Denoting them by

$$\gamma_{\text{ext}_n} := R_n^2\gamma_{pc}/N, \quad (\text{A.8})$$

we get N uncoupled differential equations from (A.7), one for each mode,

$$\begin{aligned} \ddot{\xi}_n + 2\gamma_0\dot{\xi}_n + 2\gamma_{\text{ext}n}\dot{\xi}_n + \omega_{\text{cell}}^2(1 + k_{cc}\lambda_n)\xi_n \\ = 2\sqrt{2\gamma_{\text{ext}n}}\frac{d}{dt}\text{Re}\{\mathbf{F}_g e^{i\omega_{\text{rf}}t}\}. \end{aligned} \quad (\text{A.9})$$

From (A.8) we see that the external decay rate of the π mode is given by $\gamma_{\text{ext}\pi} = \gamma_{\text{pc}}/N$ and hence the external decay rates of the same-order modes satisfy

$$\gamma_{\text{ext}n} = R_n^2 \gamma_{\text{ext}\pi}. \quad (\text{A.10})$$

4. Baseband state-space model

The eigenfrequencies of the modes in (A.9) are

$$\omega_n = \omega_{\text{cell}}\sqrt{1 + k_{cc}\lambda_n}.$$

See Fig. 7.4 in [5] for an illustration. Denote their offsets from the nominal rf frequency ω_{rf} by $\Delta\omega_n := \omega_n - \omega_{\text{rf}}$.

Let \mathbf{A}_n denote the complex envelope of the $n\pi/N$ mode with respect to ω_{rf} , i.e., $\xi_n = \text{Re}\{\mathbf{A}_n e^{i\omega_{\text{rf}}t}\}$. A slowly-varying envelope approximation of (A.9) is then given by

$$\dot{\mathbf{A}}_n = [-(\gamma_0 + \gamma_{\text{ext}n}) + i\Delta\omega_n] \mathbf{A}_n + \sqrt{2\gamma_{\text{ext}n}} \mathbf{F}_g. \quad (\text{A.11})$$

By introducing $\underline{\mathbf{A}} := [\mathbf{A}_1 \cdots \mathbf{A}_N]^\top$, $\Delta\Omega := \text{diag}(\Delta\omega_1, \dots, \Delta\omega_N)$, and $\Gamma_{\text{ext}} := \text{diag}(\gamma_{\text{ext}1}, \dots, \gamma_{\text{ext}N})$,

we can write the equations (A.11) as

$$\dot{\underline{\mathbf{A}}} = [-(\gamma_0 I + \Gamma_{\text{ext}}) + i\Delta\Omega] \underline{\mathbf{A}} + \sqrt{2\gamma_{\text{ext}\pi}} R^\top \mathbf{F}_g. \quad (\text{A.12})$$

The voltage signal \mathbf{V}_{pu} from the pickup probe is proportional to the field amplitude in cell N , i.e., $\mathbf{V}_{\text{pu}} \propto Q_N: \underline{\mathbf{A}}$ where $Q_N:$ denotes the N th row of Q . Using that $\sqrt{N}Q_N = (-1)^{n-1}R_n$ (which follows from basic trigonometry), we can write

$$\mathbf{V}_{\text{pu}} = \mathcal{C} \underline{\mathbf{A}},$$

where

$$\mathcal{C} = [c_1 \cdots c_{N-1} \ c_\pi] := \kappa_{\text{pu}} R \begin{bmatrix} (-1)^{N-1} & & & \\ & \ddots & & \\ & & -1 & \\ & & & 1 \end{bmatrix}, \quad (\text{A.13})$$

and κ_{pu} is a proportionality constant which can be assumed to be real (since the reference phase of \mathbf{V}_{pu} can be chosen freely).

Combining (A.12) with (A.13) and also including cavity-beam interaction, quantified by parameters α_n as in Section II, we have the following state-space realization of the same-order-mode dynamics

$$\dot{\underline{\mathbf{A}}} = \underline{\mathbf{A}} \mathbf{A} + \mathcal{B}_g \mathbf{F}_g + \mathcal{B}_b \mathbf{I}_b \quad (\text{A.14a})$$

$$\mathbf{V}_{\text{pu}} = \mathcal{C} \underline{\mathbf{A}} \quad (\text{A.14b})$$

where

$$\mathbf{A} = -(\gamma_0 I + \Gamma_{\text{ext}}) + i\Delta\Omega \quad (\text{A.14c})$$

$$\mathcal{B}_g = \sqrt{2\gamma_{\text{ext}\pi}} R^\top \quad (\text{A.14d})$$

$$\mathcal{B}_b = \frac{1}{2} [\alpha_1 \cdots \alpha_{N-1} \ \alpha_\pi]^\top \quad (\text{A.14e})$$

$$\mathcal{C} = \text{given by (A.13)}. \quad (\text{A.14f})$$

-
- [1] T. Schilcher, *Vector Sum Control of Pulsed Accelerating Fields in Lorentz Force Detuned Superconducting Cavities*, Ph.D. thesis, University of Hamburg, Germany (1998).
- [2] R. Ainsworth and S. Molloy, Studies of parasitic cavity modes for proposed ESS linac lattices, in *Proc. LINAC2012* (2012).
- [3] M. Ferrario, A. Mosnier, L. Serafini, F. Tazzioli, and J. Tessier, Multi-bunch energy spread induced by beam loading in a standing wave structure, *Part. Accel.* **52**, 1 (1996).
- [4] L. Doolittle, *Understanding 5-cell mode structures*, Tech. Rep. CEBAF-TN-0120 (Jefferson Lab, Newport News, VA, 1989).
- [5] H. Padamsee, J. Knobloch, and T. Hays, *RF Superconductivity for Accelerators*, 2nd ed. (Wiley-VCH, Weinheim, Germany, 2008).
- [6] T. P. Wangler, *RF Linear Accelerators*, 2nd ed. (Wiley-VCH, Weinheim, Germany, 2008).
- [7] J. Sekutowicz, Superconducting elliptical cavities, in *Proc. CERN Accel. School — RF for Accelerators* (CERN, Geneva, Switzerland, 2010).
- [8] O. Troeng, *Cavity Field Control for Linear Particle Accelerators*, Ph.D. thesis, Lund University, Sweden (2019).
- [9] O. Troeng, Energy-based parameterization of accelerating-mode dynamics (2020), arXiv:2009.14813 [physics.acc-ph].
- [10] E. Vogel, High gain proportional RF control stability at TESLA cavities, *Phys. Rev. Accel. Beams* **10**, 052001 (2007).
- [11] M. U. Liepe, *Superconducting Multicell Cavities for Linear Colliders*, Ph.D. thesis, University of Hamburg, Germany (2001).
- [12] K. Zhou, J. C. Doyle, and K. Glover, *Robust and Optimal Control* (Prentice Hall, Englewood Cliffs, NJ, 1996).
- [13] S. Skogestad and I. Postlethwaite, *Multivariable Feedback Control: Analysis and Design*, 2nd ed. (John Wiley & Sons, Chichester, UK, 2007).
- [14] H. A. Haus, *Waves and Fields in Optoelectronics* (Prentice-Hall, Englewood Cliffs, NJ, 1983).